Journal of Applied Polymer Science

Preparation of hydrophilic polysulfone membrane using polyacrylic acid with polyvinyl pyrrolidone

Nilay Sharma, Mihir Kumar Purkait
Department of Chemical Engineering, Indian Institute of Technology Guwahati, Guwahati 781039, Assam, India
Correspondence to: M. K. Purkait (E-mail: mihir@iitg.ernet.in)

ABSTRACT: This study examined the consequences of the addition of polyvinyl pyrrolidone (PVP) of different molecular weights with constant molecular weight of polyacrylic acid (PAA) on the morphology and permeation properties of polysulfone (PSF) membranes. The asymmetric polymeric membranes were prepared by phase inversion process using PSF in N-methyl-2-pyrrolidone (NMP) as a solvent. The surface structure and morphology of the prepared membranes were analyzed by field-emission scanning electron microscope (FESEM) and atomic force microscopy (AFM). The pore number, average pore size and area of pores for all the membranes were determined by permeability method. These ultrafiltration membranes were subjected to characterizations such as measurement of pure water flux (PWF), compaction factor (CF), bovine serum albumin (BSA) rejection for finding the permeability performance, whereas equilibrium water content, contact angle, porosity, hydraulic resistance, and ion exchange capacity (IEC) are measured for evaluating the hydrophilicity. Results demonstrate that the flux performance of the membranes and morphological parameters own a crucial inter-relationship with the molecular weight of PVP. The membrane pore area and pore number were found to be increased by increasing molecular weight of PVP with constant molecular weight of PAA. A detailed comparative study was done with Chakrabarty *et al.* (J. Membr. Sci. 2008, 309, 209) and found better in almost all the aspects. All the resulting parameters were compared and concluded with the fact that addition of small amount of PAA in PSF/PVP/NMP casting solution can be better than addition of PVP alone. © 2015 Wiley Periodicals, Inc. J. Appl. Polym. Sci. **2015**, *132*, 41964.

KEYWORDS: hydrophilic polymers; membranes; poly(vinyl chloride)

Received 3 September 2014; accepted 25 November 2014
DOI: 10.1002/app.41964

INTRODUCTION

Separation is an integral section of various downstream operation in chemical, petrochemical, food, biochemical, and several other related process industries. It is necessary to achieve the goals of purification, refining, enrichment and concentration of any desired product from a mixture. Efficient separation processes are also required to obtain high-value products in the pharmaceutical and food industries, to provide communities and industry with high quality water as well as to recover and remove valuable or toxic components from industrial effluents. In the present era use of membranes has become increasingly important, especially in the food processing and biotechnology industry for separation, concentration and fermentation of food products with high yield and purity.[1,2] Other than these industries membranes can be efficiently used in textile,[3] vanadium flow battery,[4] active packaging,[5] and electrodialysis[6] applications.

A variety of polymers such as cellulose acetate (CA), polyvinylidene fluoride (PVDF), polysulfone (PSF), polyacrylonitrile (PAN), polyethylene (PE), polypropylene (PP), and polyether sulfone (PES) are available for the preparation of commercial UF/MF membranes. Among these polymers, PSF is most preferable polymer for the preparation of polymeric membranes because of its good heat resistance, physicochemical stability, resistance to chlorine, oxidation, and chemical compatibility resistance over wide range of pH.[7] Other than this, solubility of PSF brings it under the category of suitable candidate for polymer blend membranes, as it is very soluble in N-methyl-2-pyrrolidone (NMP) and dimethyl acetamide (DMAc) and these solvents are further soluble in the coagulation medium which is mainly water for the preparation of asymmetric membrane. Albeit, PSF membrane has several advantages, these membranes are prone to be fouled because of its hydrophobicity, which can be resulted in declination of flux and life of membrane.[8] To overcome the problem of hydrophobicity some researchers have examined changing membrane surface properties using various methods such as plasma treatment,[9,10] coating,[11,12] UV-induced graft polymerization,[13] redox initiated grafting.[14] Although, these methods are very useful for altering the pore size and

pore size distribution of the membrane usually without internal pore modification.[15] But at the same time these methods have the drawback of required additional complicated steps. As a result research was focused on the addition of nanoparticles (NPs) and polymers within membrane matrix. Substantial literatures are available on the NP inclusion in the membrane for increasing the hydrophilicity. However, uniform distribution of NP in casting solution is actually difficult because of the agglomeration of NP and increased viscosity of the casting solution.[16] Although Nair *et al.*[17] found that the incorporated $CaCO_3$ NP (CCNP) uniformly distributed within the polymer matrix and increased membrane hydrophilicity was observed with increasing concentration of NPs. Contact angle values showed a gradual decrease from 82.81° for pure PSf/PEG membrane to 72.5° for the 10% incorporation of CCNP. On the contrary, if the NPs were getting trapped within the pores, then the flux would have decreased with increasing concentration of the NPs. This was due to the blockage of membrane pores by agglomerated NP.[18] It may be summarized from the literatures that the use of NP for increasing the hydrophilicity is not very favorable for better membrane permeability.

Blending of polymers in the casting solution is an important alternate to obtain different polymeric membranes with required properties and additional features of the process areas inexpensive and less complicated. Charged polymer,[19] surfactants,[20] and water soluble polymers[21–23] have been used to make hydrophilic UF membrane through homogeneous blending. Sinha and Purkait[21] prepared PSF membrane by using polyethylene glycol methyl ether (PEGME) of different molecular weight 550 Da, 2000 Da, and 5000 Da at constant concentration of 5 wt % as additive. The pure water flux (PWF) and hydraulic permeability were seen to enhance with increase in molecular weight of PEGME and it was observed that value of total fouling was decreased with increase in molecular weight of PEGME. Chakrabarty *et al.*[22,23] prepared PSF membrane by using PEG and PVP of different molecular weight as additive, in the case of PEG PWF was increased with increase in molecular weight of PEG, but BSA rejection was not increased in the same trend, it was highest for PEG 6000 Da. For PVP they found that with the increasing molecular weight of PVP membranes had more compact structure and consequently less PWF.

From the above literatures it may be found that although several authors have reported various additives to increase the hydrophilicity of PSF membrane, but the role of the mixture of two hydrophilic polymeric additives, i.e., polyvinyl pyrrolidone/polyacrylic acid (PVP–PAA) blend in PSF membrane has not been accounted yet. Therefore, in this work, the effect of addition of PVP–PAA blend in the casting solution of PSF membrane was studied. PAA was chosen as hydrophilic polymer additive in the present study because of its good compatibility with PVP. Membrane hydrophilicity is supposed to be increased by addition of PAA in membrane casting solution as PAA forms hydrogen bond with PVP. PVP of different molecular weight of 24,000 Da, 40,000 Da, and 360,000 Da and PAA molecular weight of 18,000 Da were taken for the preparation of PVP–PAA blend at constant concentration in casting solution of PSF membrane was investigated. Effects of PVP–PAA blend on permeation characteristic, morphology and hydrophilicity of membrane were examined and explained well. Morphology of each membrane was analyzed by scanning electron microscope (SEM) for cross-sectional view, field-emission scanning electron microscope (FESEM) for top surface and atomic force microscopy (AFM) for top surface as well as for finding different parameters such as number of pores, average radius of pores, area of pores and surface roughness parameters. The performances of the membranes were examined by water permeation and bovine serum albumin (BSA) rejection at three pH values, i.e., 4.8, 7, and 9.3.

EXPERIMENTAL

Materials and Reagents

Polysulfone (average molecular weight 30,000 Da) was supplied by Sigma-Aldrich Co. USA, and was used as base polymer in the membrane casting solution. NMP (supplied by LOBA Chemie, India) was used as solvent. PVP (average molecular weight 24,000 Da, 40,000 Da, and 360,000 Da) and Polyacrylic acid (average molecular weight of 18,000 Da) were purchased from Otto Chemie Private Limited India, were used as nonsolvent pore forming additives in the casting solution. BSA with molecular weight of 68,000 Da was purchased from Otto Chemie Private Limited, India. All the chemicals were reagent grade and used without further purification. Deionized water was taken from the Millipore system (Millipore, France), was used as nonsolvent in coagulation bath.

Membrane Preparation

Flat sheet PSF membranes were fabricated by the wet phase inversion method using different molecular weight of PVP and constant molecular weight of PAA. PVP–PAA blend (8 wt %) and NMP (78 wt %) were used as additive and solvent, respectively. The PSF concentration was taken constant at 14 wt % for all the cases. Membranes with different compositions were designated as PSF_1, PSF_2, and PSF_3 containing PVP–PAA blend in which molecular weight of PVP was 24,000 Da, 40,000 Da, and 360,000 Da, respectively, and molecular weight of PAA was taken as 18,000 Da (Table I). Figure 1 shows the reaction between PAA and PVP. The side groups of PVP are highly polar due to the incorporation of an amide bond in the five membered pyrrolidone ring. This structure is responsible for its highly hygroscopic nature. Whereas PAA is an anionic polymer and hence many of the side chains of PAA will lose their protons and acquire a negative charge. This makes PAAs polyelectrolyte, with the ability to absorb and retain water. When PVP and PAA react with each other, hydrogen bonding occurs and they become more hydrophilic in nature.[24]

The casting solution was stirred using a magnetic stirrer for 12 h at room temperature and then degassed for 24 h at room temperature for removal of air bubbles. The solution was then cast on a clean glass plate using a casting knife maintaining a uniform and constant thickness of 100 μm, in ambient conditions. Then without any delay the glass plate was immersed into the water bath (coagulation bath) at room temperature. The casted film instantaneously changed its color and converted from transparent to white after the immersion in the water bath and then separated out from the glass plate. The prepared

Table I. Composition of Casting Solution

Membranes	Additives (wt %)			PAA (wt %)	PSf (wt %)	NMP (wt %)
	PVP 24,000	PVP 40,000	PVP 360,000			
PSF_1	4.8	-	-	3.2	14	78
PSF_2	-	4.8	-	3.2	14	78
PSF_3	-	-	4.8	3.2	14	78
PSf1[23]	5	-	-	0	12	83
PSf2[23]	-	5	-	0	12	83
PSf3[23]	-	-	5	0	12	83

membrane sheets were then washed under running water to remove the additional amount of additive and then kept overnight in a deionized water bath to remove any residual solvent. Finally, the sheets were air dried at room temperature. Thereafter cutting them into the form of circular disks of diameter 0.03 m to place inside the membrane cell for filtration experiments.

Membrane Characterization

The pore size distribution and porosity are important parameters for finding the membrane performance.[25] The prepared membranes were characterized by permeation experiments and morphological analysis. The morphology of the prepared membranes was studied by microscopic observations. The performance of each membrane was evaluated in terms of ion exchange capacity (IEC) of the membranes, water contact angle (for finding the hydrophilicity of membrane), hydraulic resistance, compaction factor (CF), equilibrium water content (EWC), porosity, PWF, and percentage rejection (% R) of BSA.

Microscopic Observation. Microscopic observation was done by FESEM (Zeiss LSM 510 Meta), atomic force microscope (AFM, Agilent Technologies 5500 Scanning Probe Microscope) and scanning electron microscope (LEO 1430 VP, UK). FESEM and AFM images directly provided the visual information of the top surface and SEM provides the information about cross-sectional morphology of the membranes. Images were taken with acceleration voltages of 10 kV and 3.50 kV for SEM and FESEM, respectively, after the samples were double coated with thin gold layer (for about 135 s). The skin layer thickness as well as pore size on the membrane surface was measured with the help of image J[26] and WSxM[27] softwares. These images directly provide the top layer visual information as well as cross-sectional information of the membranes. A number of FESEM, AFM, and SEM images were taken at different magnification for top surface and cross-section of the prepared membranes.

Permeability Method. The number of pores and average pore size of the fabricated membranes were determined by permeability method.[7] In this method the flow of a solvent through a porous membrane can be described in terms of a pore flow model which assumes that the pores are ideally cylindrical in shape and aligned normal to the membrane surface. Hagen-Poiseuille equation may be used to describe the volumetric flux through these pores.

$$J_v = \frac{\varepsilon_m d_p^2 \Delta P}{32 \mu \tau l_p}{}_p \quad (1)$$

where ε_m is the surface porosity of membrane, d_p is diameter of the pore, $\triangle P$ is pressure difference, μ is liquid viscosity, τ is the pore tortuosity (for cylindrical perpendicular pores, the tortuosity is equal to unity), and l_p is the length of pores or almost equal to the thickness of membrane. Flow per unit membrane area or the flux, is the sum of all the flows through the individual pores (N pore) and can be given by:

$$J = \frac{N.\pi d^4 \Delta P}{128 \mu l_p} \quad (2)$$

For the membranes having equal pore area and porosity, the inverse of square of the pore diameter is proportional to the number of pores cm^{-2}.

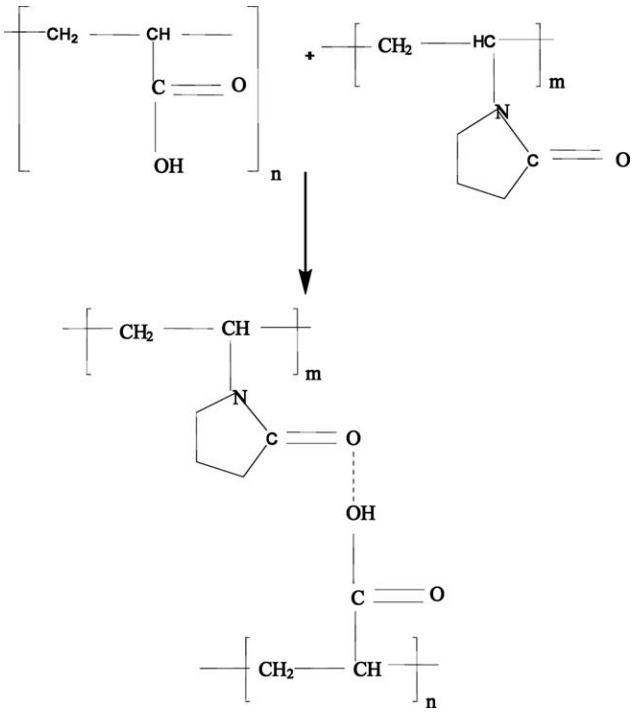

Figure 1. Reaction between polyacrylic acid and polyvinyl pyrrolidone ($n \sim 25$ and $m \sim 216$).

$$N = \frac{4.\varepsilon}{\pi d^2} \quad (3)$$

The mean pore radius r_{av} was calculated as:[28]

$$r_{av} = \frac{\sum N_{ij}.r_{ij}}{\sum N_{ij}} \quad (4)$$

where N_{ij} is the pore number that have radius between r_i and r_j per unit area of the membrane surface. This method has some advantages like experimental simplicity, particularly when liquids are used. However, pore geometry consideration is very necessary in this method and it is the major limitation of this method. But the information found from this method may be useful for the comparison of different membranes.

Permeation Experiments. All the unstirred batch experiments were carried out at room temperature ($25 \pm 2°C$) in a dead-end, stainless steel cell with a diameter of 3×10^{-2} m, volume 400 mL and effective membrane filtration area of 7.065×10^{-4} m^2 fitted with Teflon coated O-ring. Nitrogen gas was used to pressurize the cell to an operating pressure of 100 kPa after the compaction of membrane at 240 kPa. Inside the cell, a flat circular membrane was kept over a base support. The permeating solution was collected from the bottom of the cell. Prepared membrane was compacted with deionized water for 4 h at a transmembrane pressure of 240 kPa which was higher than the maximum operating pressure for this study. The water permeation flux was collected at every 30-min interval until the flow stabilization through the membrane was achieved. The ratio of initial pure water flux ($PWF_{initial}$) to steady state pure water flux ($PWF_{steady\ state}$) was used for calculating the CF

PWF and Hydraulic Permeability (P_m). Membrane hydraulic permeability is an important parameter for membranes used in pressure driven separation processes. PWF was calculated by allowing deionized water to move across the compacted membrane. Flux values of pure water at different transmembrane pressures (up to 240 kPa) were calculated under steady state condition with the help of following equation:

$$J_w = \frac{Q}{A\Delta t} \quad (5)$$

where J_w is the PWF (L m^{-2} h^{-1}), Q is the volume of water permeated (L), A is the effective membrane area (m^2), Δt is the permeation time, and P_m (L m^{-2} h^{-1} kPa^{-1}) is evaluated from the slope of the plot of J_w vs. P. Hydraulic permeability was measured using following equation as:[21]

$$P_m = \frac{J_w}{\Delta P} \quad (6)$$

EWC, Porosity, and Hydrophilicity. EWC is basically related to the porosity of membrane. It also depicts the hydrophilicity or hydrophobicity of the membranes. EWC at room temperature was obtained as:

$$\mathrm{EWC}(\%) = \frac{(W_w - W_d)}{W_w} \times 100 \quad (7)$$

The membrane porosity was determined as:[22]

$$\mathrm{Porosity} = \frac{(W_w - W_d)}{\rho_w \times V} \quad (8)$$

where W_w and W_d are the weight of membrane in wet and dry conditions, respectively. V is volume of the membrane and ρ_w is the density of water. Weight of wet membranes was taken on electronic weighing machine after soaking the surface water using a clean tissue paper. Vacuum oven was used for drying the wet membranes and were dried for a period of 24 h at a temperature of about 50–55°C and over again they were weighed in dry state. For calculating the volume of membrane, thickness of membranes was assessed by SEM image at different places and the average was taken for analysis. The error was found within the range of 2–3%. Static contact angle between the membrane films and deionized water was measured at room temperature and at ambient condition using a digital camera (sony cyber shot) and a goniometer. Contact angle is an important parameter for finding the hydrophilicity of membranes. Farbod and Rezaian[29] had also measured contact angle with the same technique. For measuring the contact angle, membrane pieces of rectangular shape of about 4 cm × 2 cm area was prepared by cutting the membrane sheet and then these samples were fixed at glass plates using the tape. Then, a drop DI water (~20 μL) was placed on the surface with the help of a micropipette.[21]

Ultrafiltration Experiment

Ultrafiltration experiments were carried out in the batch cell explained in the previous section to study the effect of molecular weight of PVP with PAA on permeate flux and solute separation behavior of the prepared membranes. The protein, BSA, was used for the filtration experiments. Solution was prepared by dissolving BSA in deionized water and the concentration of solution kept constant at 1000 mg L^{-1} for all the filtration experiments. The pH of protein solution acts as a key factor in protein-membrane interaction.[30] The pH of the BSA solution (molecular weight 68,000 Da) was taken approximately at three values: 4.8 [i.e., at isoelectric point (IEP)], 7 (i.e., neutral state), and 9.3 (i.e., basic condition). Then the membrane was fixed in the membrane cell, the cell was first filled with deionized water. Initially, each membrane was pressurized for 60 min at 157 kPa, then the pressure was reduced to the operating pressure of about 100 kPa and the water flux (J_{w1}) was noted. Afterward cell was emptied and refilled with 1000 mg L^{-1} BSA solution; the flux was noted as (J_p). Then the BSA rejection ratio was measured by the following equation:

$$R\% = \frac{(1 - C_p)}{C_f} \times 100 \quad (9)$$

where C_f and C_p are the concentrations in the feed and permeate in mg mL^{-1}, respectively. After 2 h of ultrafiltration, the membrane was cleaned with deionized water by back-washing and water flux was measured (J_{w2}). UV–vis spectrophotometer (Perkin-Elmer Precisel, Lamda-35) was used for obtaining the BSA concentration in permeate; concentration was measured spectro-photometrically at wavelength of 280 nm. Membrane fouling causes flux loss ($J_{w1} - J_p$). To examine the antifouling property of the membrane, Wang *et al.*[31] defined some ratios to explain the fouling process. The first ratio is total resistance R_t,

which is the degree of total flux deficit caused by total fouling. R_t was measured by the following equation:

$$R_t = 1 - \left(\frac{J_p}{J_{w1}}\right) \quad (10)$$

R_{ir} and R_r are two additional ratios. Where R_{ir} is irreversible fouling and R_r is reversible fouling. R_r and R_{ir} were calculated by the following equation:

$$R_{ir} = \frac{(J_{w1} - J_{w2})}{J_{w1}} \quad (11)$$

$$R_r = \frac{(J_{w2} - J_p)}{J_{w1}} \quad (12)$$

Reversible fouling occurs due to the reversible BSA adsorption on the membrane surface, which can be eliminated by hydraulic cleaning whereas irreversible fouling caused by irreversible BSA adsorption may be inside the pores, which can difficult to be removed by hydraulic washing. Thus, R_t is the sum of R_r and R_{ir}.

$$R_t = R_r + R_{ir} \quad (13)$$

The data obtained from ultrafiltration of BSA protein through different membranes are analyzed in successive section.

Ion Exchange Capacity

The IEC of the PSF–(PVP–PAA) membranes was determined by the back titration method. Initially, 0.3 g PSF–(PVP–PAA) membrane samples were equilibrated with 50 mL 0.01 *M* HCl standard solution for 24 h, at 30°C in orbital shaker for achieving complete equilibrium, followed by back titration of 0.01 *M* NaOH standard solution with phenolphthalein as the indicator. The 50 mL 0.01 *M* HCl standard solution was used as the blank sample for the control experiment. The measured IEC of the PSF–(PVP–PAA) membranes were calculated by the following equation:[32]

$$\text{IEC} = \frac{(V_b - V_s) C_{\text{HCL}}}{W_{\text{dry}}} \times 1000 \quad (14)$$

where V_b and V_s are the consumed volumes (L) of the NaOH solution for the blank sample and the PSF–(PVP–PAA) membrane sample, respectively, C_{HCl} is the concentration of HCl solution (M), and W_{dry} is the mass (g) of dry membrane sample.

Comparison of Resistances with Respect to the total Resistance

For finding the long term steadiness and for evaluating the efficacy of the cleaning procedures of membrane, different type of resistances such as membrane resistance (R_m), gel layer resistance (R_g), and resistance due to pore blocking (R_{PB}) were also calculated using the resistance model:[33]

$$J_{\text{water}} = \frac{P_T}{R_m} \quad (15)$$

where J_{water} is PWF, P_T is the pressure, and R_m is membrane resistance.

$$J_{\text{water}} = \frac{P_T}{(R_m + R_{\text{pb}})} \quad (16)$$

where R_{pb} is the resistance due to fouling or pore blocking.

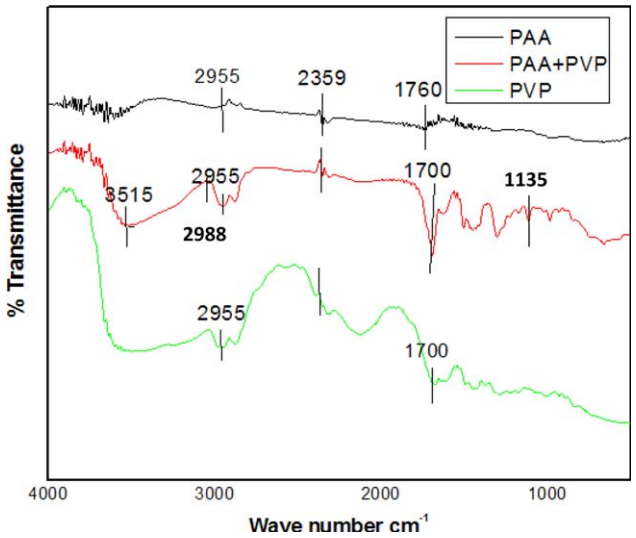

Figure 2. FTIR-ATR spectra of PAA, PAA-PVP blend, and PVP. [Color figure can be viewed in the online issue, which is available at wileyonlinelibrary.com.]

$$J_{\text{water}} = \frac{P_T}{(R_m + R_{\text{pb}} + R_g)} \quad (17)$$

where R_g is gel layer resistance. It is a function of operating parameters and physical properties; it is also used for accounting boundary layer and concentration polarization.

RESULTS AND DISCUSSION

FTIR-ATR Spectroscopy Analysis of PVP–PAA Blend

Figure 2 shows the FTIR spectra of PAA, PVP, and PVP–PAA blend. FTIR analysis shows that the complexes were formed through hydrogen bonding between the carboxyl groups of the PAA and the carbonyl groups of the PVP. As shown in Figure 2, peaks at 2988 cm^{-1} and 1760 cm^{-1} are characteristic peaks of C–H stretch and C═O carboxylic acids, respectively, present in PAA. The peak at 1115 cm^{-1} and 3515 cm^{-1} are characteristic peaks of C–N in aromatic amine and –OH group present in PVP–PAA blend. Another peak at 2955 cm^{-1} is due to C–H stretching in blend. Peak at 1700 cm^{-1} shows the presence of C═O group in the PVP.[24]

Morphological Study

Phase inversion method in wet process was used for the preparation of PSF/PVP–PAA/NMP blended membranes. For finding the size, number and area of pores as well as for determining surface roughness parameters AFM images were taken. Quantitative information about surface morphology of the prepared membranes of different composition was examined by high-resolution FESEM also. Higher magnification was required for top surface images to find the size of pores, so these images were taken by FESEM. On the other hand, cross-sectional morphologies of the prepared membranes were obtained through SEM analysis. In the case of cross-sectional morphology lower magnification was sufficient as only pore structure was observed.

SEM Analysis. Figure 3(a) shows the SEM images of the cross-sectional view of different membranes prepared with three

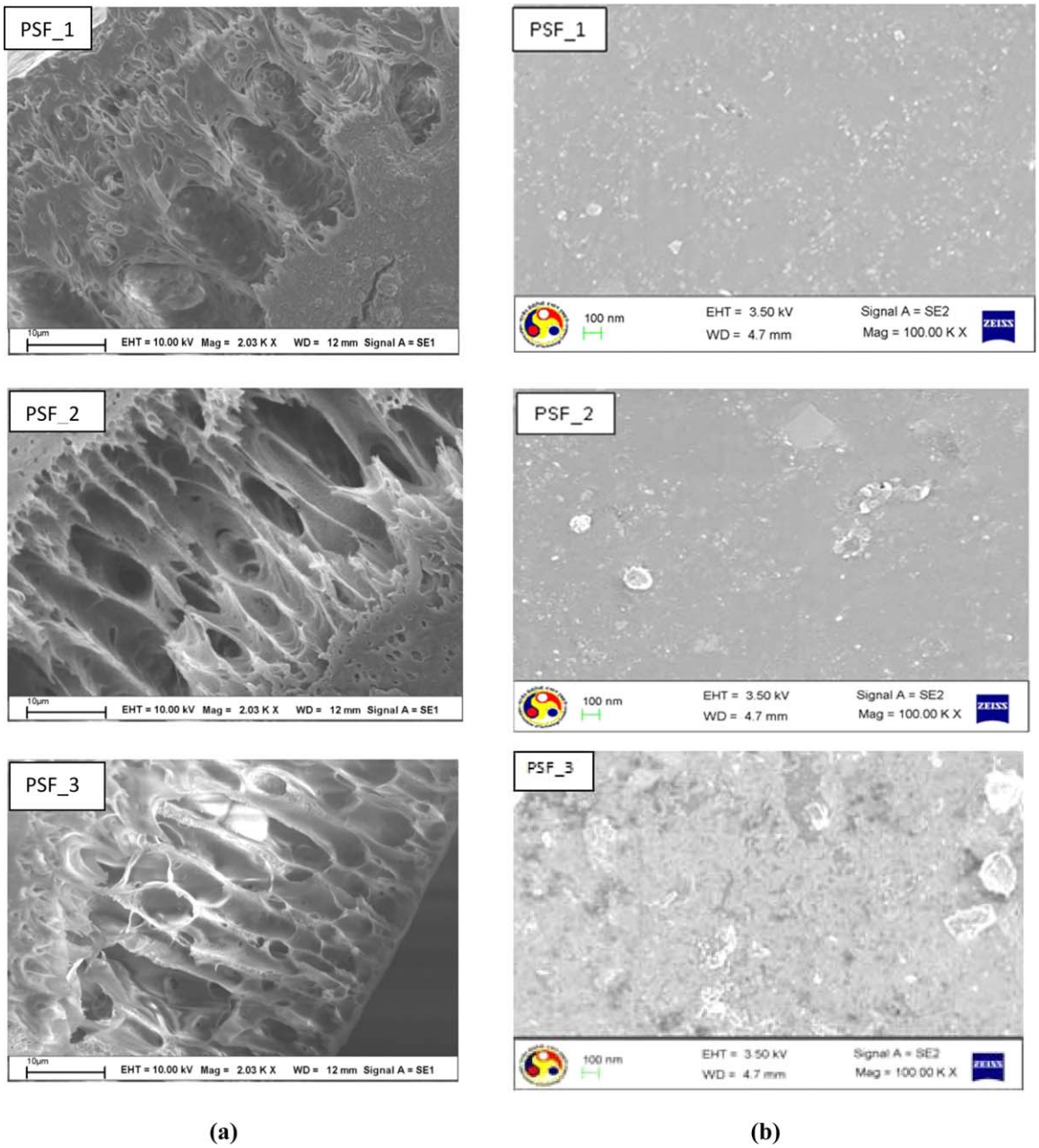

Figure 3. (a) SEM images of membrane cross-section and (b) FESEM images of membrane top surface. [Color figure can be viewed in the online issue, which is available at wileyonlinelibrary.com.]

different molecular weight of PVP with PAA in this study. From the images it can be seen that membranes so prepared were asymmetric porous structure. General structure shows a dense top layer and a porous sublayer, which was very similar for all the membranes. The porous sublayer seems to have finger-like structure. Similar observation was depicted by Chakrabarty *et al.*[23] for the system of PSF as base polymer with DMAc and NMP as solvent using different molecular weight of PVP as additive. Because of high interactive affinity of NMP for water, instantaneous demixing occurs, further leading to the creation of finger like cavities in the sublayer of the prepared membranes.[7] Sinha and Purkait[21] also found the same result, for the system of PSF as polymer using NMP as solvent with different molecular weight of PEGME as additive.

FESEM Analysis. FESEM images for the top surface (air-side) of different membranes are shown in Figure 3(b). The top surface formation was probably due to the spinodal demixing. This is due to the fact that during formation of top layer the diffusion process was so fast for the polymer solution to become highly unstable and cross the spinodal curve.[34,35] This provides a top surface with much better interconnected pores. The interconnected pores can be taken as a continuous PSF lean (i.e., PVP–PAA rich) phase intertwined by a continuous PSF rich

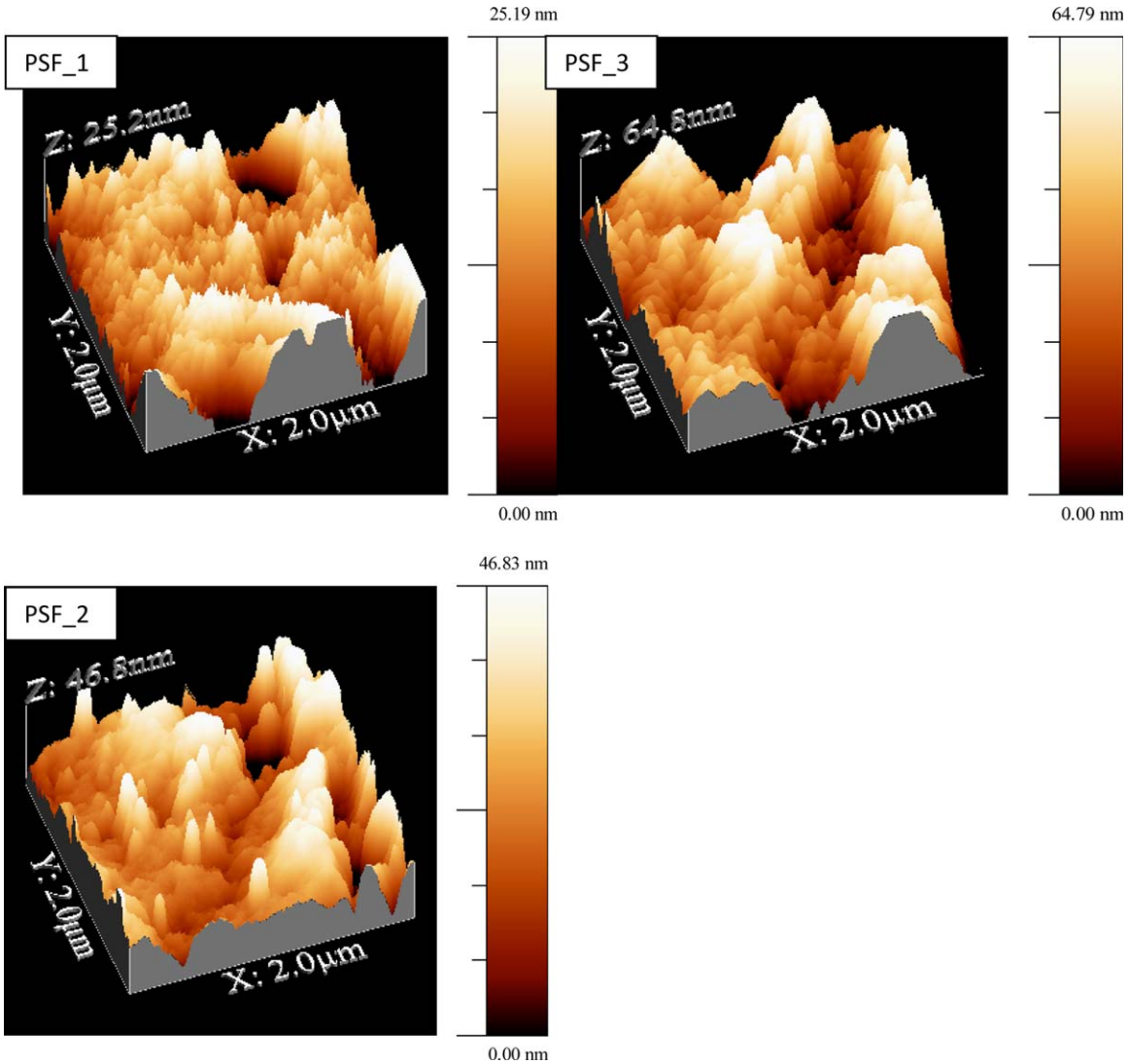

Figure 4. Three dimensional AFM surface images of PSF_1, PSF_2, and PSF_3. [Color figure can be viewed in the online issue, which is available at wileyonlinelibrary.com.]

(i.e., PVP–PAA lean) phase which was responsible for the formation of the membrane matrix.

Few round formations in Figure 3(b) depicted that although homogeneous solution was made for membrane preparation but still few polymeric particles remained insoluble in the casting solution. Image J software was used for determining the pore size from FESEM results, shown in Figure 3(b) and again confirmed by AFM images shown in Figure 4 for various membranes. Average pore size was calculated as 47.12 nm, 45.85 nm, and 40.65 nm for PSF_1, PSF_2, and PSF_3, respectively, which confirms that the membranes are in UF range.

AFM Analysis. AFM was used to analyze the surface morphology and roughness of the membranes. Small squares of membranes (approximately 1 cm^2) were cut and analyzed. The membrane surface was examined in a scan size of 2 μm × 2 μm. Figure 4 shows the AFM images of the membranes. Root mean square (RMS) roughness (S_q), average roughness (S_a), and average height (S_z) were measured. RMS roughness is increasing with increase in molecular weight of PVP. It was measured as 5.81 nm, 10.36 nm, and 15.70 nm for PSF_1, PSF_2, and PSF_3, respectively. It may be due the fact that number of pores on the surface was increasing (i.e., porosity increasing) with increase in molecular weight of PVP. Table II shows the surface roughness parameters. The contact angle decreases with increasing molecular weight and was measured as 74°, 48°, and 32° for PSF_1, PSF_2, and PSF_3, respectively. It indicates increasing hydrophilicity with increase in molecular weight of PVP as molecular weight of PAA was taken constant in this study.

Permeability Method. The pore size, number of pores and pore area for each membrane were determined using eqs. (1–3). At different pressure the PWF was varying. The flux was higher at higher pressure and pore size was changing at different pressures, as by applying more pressure smaller pores were opened. However, pores smaller than 2 nm are difficult to be measured by this method because of the pressure limitation. Lesser

Table II. Surface Roughness Parameters of the Membranes

Membrane	RMS roughness, S_q (nm)	Average roughness, S_a (nm)	Average height, S_z (nm)
PSF_1	5.81	4.52	12.70
PSF_2	10.36	8.14	23.75
PSF_3	15.70	12.68	32.37

number of bigger pores mainly governs the total membrane performance by raising the permeability. Increase in flux with increase in radius of pore can be explained by eq. (1), i.e., from the Hagen-Poissuille equation which depicted that the flow through a membrane proportional to the fourth power of the radius of pore. Table III depicts the results of permeation method. It was observed that with increase in molecular weight of PVP number of pores for all the membranes increased, consequently more porous membrane were obtained. Number of pores per unit area (N_t) were found to be increased from 3.1 $\times$ 10^9 to 16 $\times$ 10^9 and these results were compared with Chakrabarty *et al.*[23] and found better in all aspects.

Permeation Experiments

PSF/PVP–PAA/NMP blended membranes were examined by permeation behavior to observe the effect of PVP–PAA blend and different molecular weight of PVP. The membranes were characterized in terms of CF, hydraulic permeability, and PWF. Effects of various parameters on EWC, hydraulic resistance and porosity were studied. Finally, the membranes were subjected to study for rejection as well as permeate flux behavior with protein (BSA) at different pH. Results have been reported in subsequent sections.

Effect of Molecular Weight of PVP with PAA on CF. CF is an important parameter for relating the structure of the membrane, especially for the membrane sublayer. Higher the CF, the membrane is more prone to be compacted because of the presence of large number of macrovoids in the sublayer. The effect of compaction time on PWF for all the membranes is shown in Figure 5. For all the membranes, PWF is initially seen to decline sharply with time due to compaction and finally attain a steady

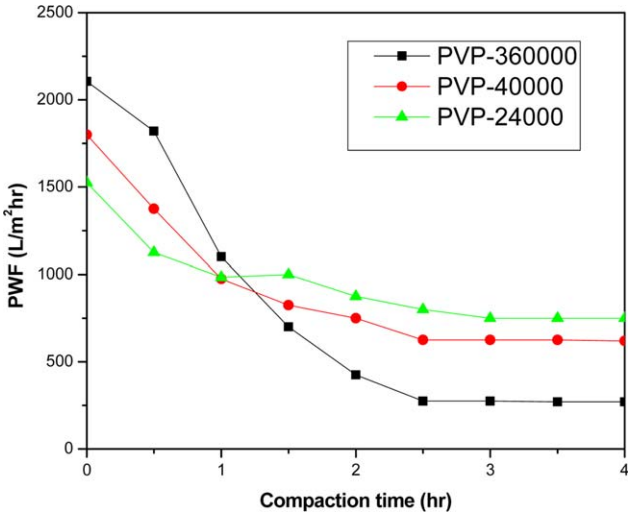

Figure 5. Flux profile during compaction. [Color figure can be viewed in the online issue, which is available at wileyonlinelibrary.com.]

state after around 3 h. This was due to the fact that the walls of the pores become denser, closer and uniform resulting reduction in pore size in addition to the flux for the duration of compaction.[7] From the figure it was found that the steady state PWF decreases with increase in molecular weight of PVP. For example, the steady state flux decreases from around 695 L m^{-2} h^{-1} to 242 L m^{-2} h^{-1}, when molecular weight increases from 24,000 Da to 360,000 Da. The CF for the membranes is presented in Table III. It is seen that for PSF/NMP/PVP–PAA membranes (i.e., PSf_1, PSf_2, and PSf_3), the CF increases from 2.06 to 10.42 with increase in molecular weight of PVP. Similar observations were obtained by Chakrabarty *et al.*,[23] steady state PWF was decreased from 355.4 L m^{-2} h^{-1} to 118.5 L m^{-2} h^{-1} and CF increased from 1.76 to 6.67 for similar molecular weight of PVP, in their study. So, in the present study results were found better than.[23] This may be due to the fact that addition of two additives into the casting solution can either more enlarge or extra suppress the macrovoids in the membrane sublayer depending on their molecular weight as well as the type of solvent used.[36] In the present study, it is possible that for PSF/NMP/PVP–PAA system, increase in molecular

Table III. Values of Some Characterization Parameters of All Membranes

Membrane	PSF_1	PSF_2	PSF_3	PSf1[23]	PSf2[23]	PSf3[23]
Equilibrium water content EWC (%)	51.23	62.4	74.32	46.8	58.2	73.4
Hydraulic resistance, R_m (m^2 h kPa L^{-1})	0.35	0.48	1.01	0.46	1.2	1.58
PWF (L m^{-2} h^{-1}) at 240 kPa	695.65	511.58	242.45	355.4	152.9	118.5
Compaction factor, CF	2.06	3.42	10.42	1.76	3.0	6.67
Contact angle (deg)	74	48	32	-	-	-
Porosity	0.38	0.49	0.61	-	-	-
Ion exchange capacity (IEC)	2.408	1.363	0.733	-	-	-
BSA rejection % at pH 9.3	41.12	45.5	64.52	40	-	62
Number of pores N_t $\times 10^{-9}$ (cm^{-2})	3.1	5.01	16	2.6	4.1	9.8
Area of pores A_t $\times 10^3$ (cm^2)	2.43	3.31	7.36	1.17	1.23	3.1

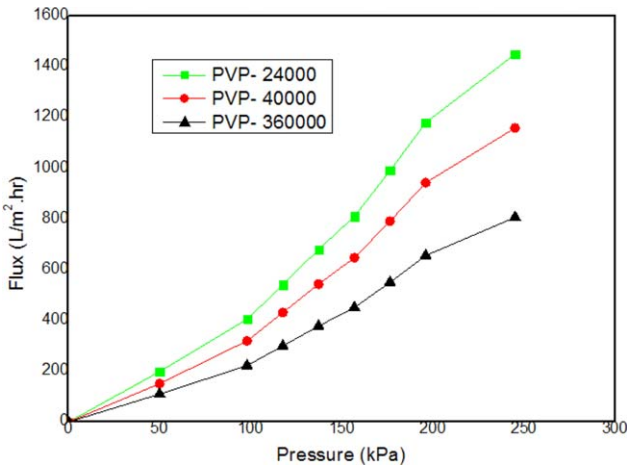

Figure 6. Effect of transmembrane pressure on PWF. [Color figure can be viewed in the online issue, which is available at wileyonlinelibrary.com.]

weight of PVP has resulted in a membrane with a highly porous substructure due to presence of higher number of macrovoids which may be bigger than the pores formed by PVP alone. This fact can also be understood from the SEM figures [Figure 3(a)]. This may be because of the reason; some PVP–PAA molecule present in the membrane matrix remained inside and gets swelled. Thus, slightly bigger pores were formed.

Effect of Molecular Weight of PVP on PWF and Hydraulic Permeability. Figure 6 depicts the effect of molecular weight of PVP on PWF at different transmembrane pressures. It was seen that within the range of 0–240 kPa, PWF [calculated using Eq. (5)] increases almost linearly with increase in transmembrane pressure, for all the membranes. It was also found that the PWF decreased with increase in molecular weight of PVP at a specific pressure which supports with the findings of the compaction study (Figure 5). For example, at 137 kPa, the PWF decreases from around 501 L m^{-2} h^{-1} to 275 L m^{-2} h^{-1} when molecular weight of PVP increases from 24,000 Da to 360,000 Da.

Hydraulic resistance (R_m) is calculated from the inverse of the slope of the plots of Figure 6. It was observed that hydraulic resistance (R_m) was increased with increase in the molecular weight of PVP. R_m for PSf/NMP/PVP–PAA system was calculated as 0.35, 0.48 and 1.01 (m^2 h kPa L^{-1}) for PSF_1, PSF_2, and PSF_3, respectively. Similar type of results were found by Chakrabarty *et al.*[23] They calculated R_m for PSf/NMP/PVP system as 0.46, 1.2, and 1.58 (m^2 h kPa L^{-1}) for PSf1, PSf2, and PSf3 (Table I), respectively, for same molecular weight of PVP.

The increase in hydraulic resistance and hence the decline in flux with increase in molecular weight of PVP may be credited to the reduction in pore size at the top layer with higher molecular weight PVP. According to the literature,[37,38] although most of the additives are sluiced away during washing and coagulation time, but it is always not possible to remove the additives completely from the membrane matrix and it becomes more and more difficult with increase in molecular weight of additives, i.e., PVP. Therefore, small amount of PVP, which is hydrophilic in nature may possibly to be entangled inside the membrane matrix lastingly. In this study, it may be possible that swelling of those trace amount of PVP–PAA molecules predominantly took place because of its hygroscopic and hydrophilic nature. This was happened due to pore blocking and consequently reduction in flux.[24] Swelling rate also increases with increase in molecular weight of PVP, later it caused the increased pore blocking. Higher molecular weight of PVP 360,000 Da containing membrane (PSF_3) had more suppressed sublayers which can be seen in Figure 3(a) that possibly to offer more resistance to water permeation consequential in lower flux. Comparison of present membrane morphology with literature[23] is presented in Table III and explained subsequently.

Membrane Characterization by EWC, Porosity, and Hydrophilicity

Effect of Molecular Weight of PVP with PAA on EWC. The EWC of all the membranes was calculated using Eq. (7) and presented in Table III. It has a strong relationship with PWF. It is an influential parameter for characterization of membrane and it was found from the calculations that increase in molecular weight of PVP, EWC of the membrane increases. The EWC for PVP 24,000, PVP 40,000, and PVP 360,000 were 51.23%, 62.4%, and 74.32%, respectively. This increasing trend confirms the presence of increasing number of pores in the membrane with increase in the molecular weight of PVP (Table III). The pores on the surface as well as cavities in the sublayer are responsible for accommodating water molecules in the membrane.[39] Chakrabarty *et al.*[22,23] reported the similar trend with PSf/NMP/PEG and PSf/DMAc/PVP and membranes. Comparison with those literatures number of pores was found to be increased by addition of PAA in the membrane matrix. This may be because of the fact that water molecules may diffuse into the PVP–PAA molecule during immersion of membrane in water (wet phase inversion method) and disturb the network. Hydrogen bonds between PVP and PAA may have been broken and some PAA molecule came out to the surface of membrane caused more pores on the membrane surface.

Effect of Molecular Weight of PVP on Porosity and Hydrophilicity. Hydrophilicity and porosity of the membrane are important parameters in membrane permeation and separation processes and it is closely related to the morphology and PWF of the membrane. Surface hydrophilicity is mainly described by the contact angle measurement.[29] In general term, smaller the contact angle values higher the hydrophilicity. Porosity of the membranes was measured using Eq. (8). Calculated values of porosity and contact angle of membranes with different molecular weight of PVP are shown in Table III. It can be found from Table III that contact angle decreases and porosity increases with the increase in molecular weight of PVP. The contact angle for PVP 24,000 is 74°, for PVP 40,000 is 48°, and for PVP 360,000 is 32°. Similarly, Porosity for PVP 24,000, PVP 40,000, and PVP 360,000 is 0.38, 0.49, and 0.61, respectively. The porosity variation can be explained on the basis of kinetic and thermodynamic contemplation. With the addition of additives into the casting solution mainly two effects occur. Firstly, it causes thermodynamic improvement in the phase separation due to the reduced miscibility of the casting solution in nonsolvent; this results in the immediate demixing. Secondly, it creates kinetic hindrance against phase separation due to increased

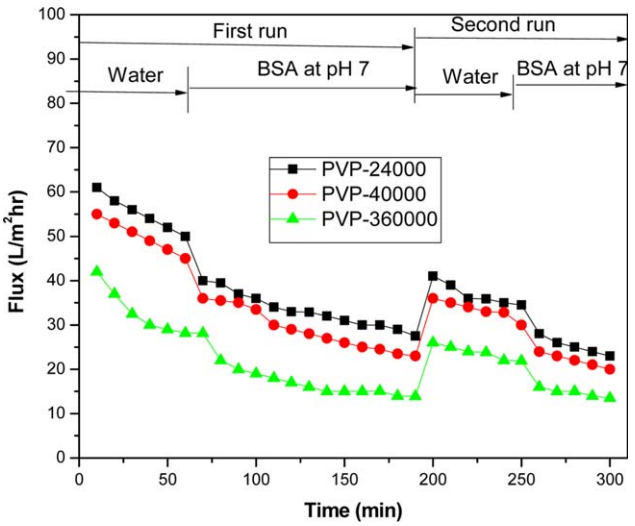

Figure 7. Time dependent flux of membrane during ultrafiltration. [Color figure can be viewed in the online issue, which is available at wileyonlinelibrary.com.]

viscosity of the solution; thus concluding in delayed demixing.[7] The viscosity of casting solution was measured as 0.136 Pa s, 0.151 Pa s, and 0.176 Pa s for PSF_1, PSF_2, and PSF_3 membranes, respectively. With increase in viscosity, the ratio of nonsolvent inflow to solvent outflow increases, which according to the theory recommended by Young and Chen[40] consequences in a more porous membrane. The increase in membrane porosity with higher molecular weight of PVP was possibly due to decrease in miscibility of the casting solution in water. This in turn caused thermodynamic improvement in the demixing of casting solution. The small amount of PVP–PAA molecules left within the membrane matrix can be a cause of hydrophilic behavior of membrane. Consequently, the entrapment of PVP–PAA molecules in membrane matrix improves the hydrophilic properties of membrane. Higher molecular weight of PVP tends to retained more residual of PVP–PAA and reduced contact angle.

Ultrafiltration of BSA

Other than transmembrane pressure, the flux characteristics and rejection of the membranes mostly depend on the structure of the membrane and the properties of the feed solution. So, the prepared UF membranes were also characterized by measuring flux in permeation experiment and rejection by means of BSA solution (1000 mg L^{-1}). To investigate the fouling behavior, membranes were cleaned by back washing after BSA solution ultrafiltration, and the PWF of the cleaned membranes was measured. Figure 7 shows the time-dependent flux of membranes during ultrafiltration. It can be seen that before UF of the BSA solution, PWF (J_{w1}) changes marginally, but it decreased inordinately at the first run of BSA solution ultrafiltration. It happened because of the adsorption or deposition of protein molecules on surface of membrane at the first BSA ultrafiltration operation.[2,16,41] After some time of operation it reaches to equilibrium, so that a relatively steady flux (J_p) was achieved in the final run of BSA ultrafiltration.

Reversible and Irreversible Fouling. Membrane fouling can be classified in two types viz. reversible and irreversible. Reversible adsorption and deposition of protein results in reversible fouling that can be removed by hydraulic cleaning only. While irreversible protein deposition or adsorption causes irreversible fouling that can merely be eliminated by enzymatic degradation or chemical cleaning.[34] For finding these fouling values, pH of 7 was maintained throughout the experiments. Effect of molecular weight of PVP on total fouling (R_t), reversible fouling (R_r), and irreversible fouling (R_{ir}) is summarized and depicted in Figure 8. It may be recognized that R_t increases from 0.75 to 0.88 with increase in molecular weight of PVP from 24,000 Da to 360,000 Da. The higher value of R_t indicates higher total flux loss, resulting in more protein adsorption or deposition on the membrane surface.[34] Figure 8 also shows that membrane containing higher molecular weight PVP has higher value of R_{ir}. This may be because of the fact that the membrane containing higher molecular weight of PVP has higher value of continuous protein adsorption and deposition on the membrane and initial water flux could not be regained by a simple cleaning methods using deionized water.

Effect of Molecular Weight of PVP. Figure 9 depicts the result of the addition of different molecular weight of PVP in membrane casting solution on the BSA rejection at different solution pH of 4.8, 7, and 9.3. It can be seen from the figure that with the increase in molecular weight of PVP from 24,000 Da to 360,000 Da, the rejection increases from 65.5% to 87.5%, 35% to 66%, and 5% to 49% when pH of BSA solution was 4.8, 7, and 9.3, respectively. The protein rejection by ultrafiltration membranes can be explained with the concept of protein adsorption and subsequently pore contraction, as a result of both electrostatic and hydrophobic contacts between the membrane surface and the protein molecules.[42,43] Denser top layer of higher molecular weight of PVP with PAA also offered

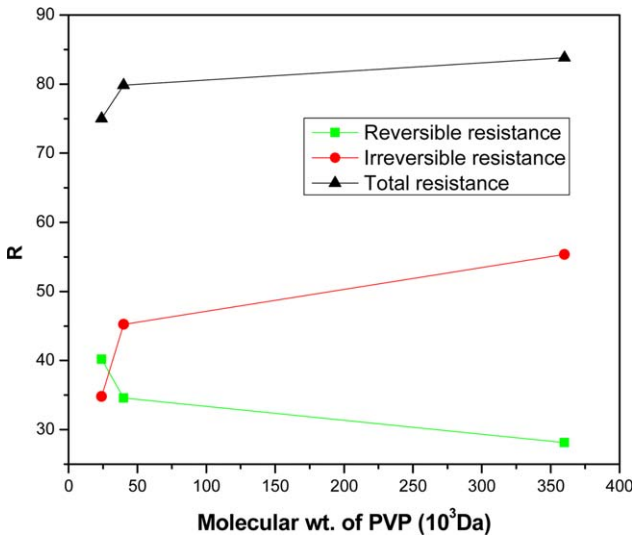

Figure 8. Summary of R_t, R_r, and R_{ir} of different membranes. [Color figure can be viewed in the online issue, which is available at wileyonlinelibrary.com.]

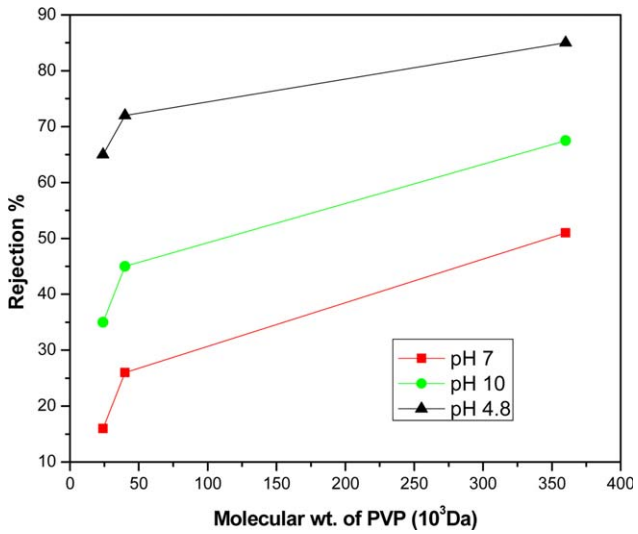

Figure 9. Effect of molecular weight of PVP on BSA rejection at 100 kPa and concentration of BSA was 1000 mg L^{-1} for 2 h UF. [Color figure can be viewed in the online issue, which is available at wileyonlinelibrary.com.]

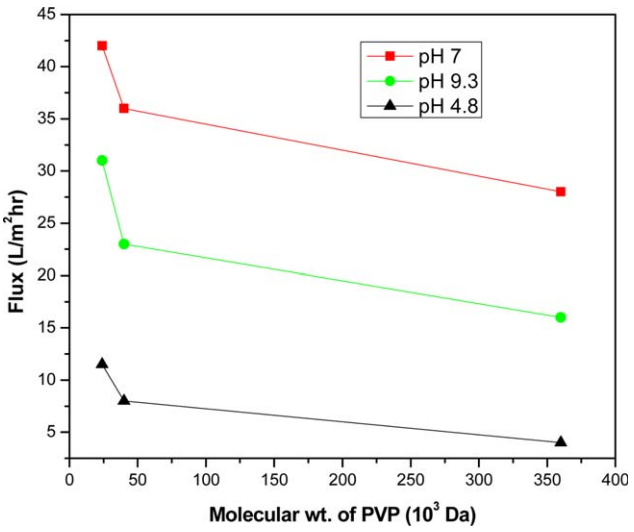

Figure 10. Effect of molecular weight of PVP on BSA flux at different pH at 100 kPa and concentration of BSA was 1000 mg L^{-1} for 2h UF. [Color figure can be viewed in the online issue, which is available at wileyonlinelibrary.com.]

greater resistance toward the protein molecule for all pH values caused increasing tendency in percentage rejection.

Figure 10 shows the average flux using BSA solution during 2 h ultrafiltration with respect to the molecular weight of PVP in membrane casting solution. The pH of the BSA solution was maintained at 4.8, 7, and 9.3. It may be seen from the figure that with increase in molecular weight of PVP from 24,000 Da to 360,000 Da, the flux slowly decreases from 12 to 2.2 L m^{-2} h^{-1}, 47.5 to 28 L m^{-2} h^{-1}, and 31 to 16 L m^{-2} h^{-1} when pH of BSA solution was 4.8, 7, and 9.3, respectively. This decreasing fashion of flux, irrespective of the pH of BSA, might be due to the formation of membranes with higher pore density.

Effect of pH of BSA. The BSA rejection strongly depends on pH. Flux was minimum and rejection was maximum at IEP of BSA solution. At IEP (i.e., at pH 4.8), BSA molecules have no charge and they are least soluble at its IEP. The BSA molecules rested in its most compact size when get deposited on the membrane surface and form slightest permeable layer.[42–44] This compact layer is accountable for least flux and highest BSA rejection. At neutral pH, BSA molecules have net negative charge and expand because of electrostatic repulsion; these effects would likely to give an additional permeable deposited layer and should give a lower rejection and higher flux. IEC is an important tool for finding the information regarding charge density in the membranes and it affects their pH responsive behavior by BSA protein and fouling behavior as well. Table III shows the IEC of different membranes. IEC of membrane PSF_1, PSF_2, and PSF_3 were 2.4, 1.36, and 0.73, respectively. More ionization of PAA, present in membrane matrix of PSF_1 may be the reason of highest IEC value for PSF_1. Membrane with lower molecular weight of PVP have free PAA molecule, however PAA concentration was kept constant for all three membranes. Change in BSA solution flux with pH can be explained by protonation and deprotonation capability of PAA, as its acid dissociation constant pKa is about ~4.9, carboxylic group of PAA deprotonated to carboxylate ions. These carboxylate ions provide high charge density in the PVP–PAA blended membranes, which results in expansion of PVP–PAA molecule and expansion of molecule blocks the membrane pores to some extent. Again on additional increment of pH, there is more loss of flux, which was because of the electro viscous effect.[44] This physical phenomenon occurs when an electrolyte solution is passed through a narrow capillary or pore with charged surface.[45] In this study at pH above 7, i.e., at pH 9.3 membranes and permeating liquid both have negative charge. As the pH increases, more negative charge comes to the permeating liquid, so membrane repels the permeating liquid from passing through the membrane pores and that feel more revulsion from the membrane and consequently more loss of flux. Higher rejection and lower flux at pH 9.3 compared to pH 7 can also be explained by Coulomb's law. During BSA (solute) separation, membrane offers some resistances and these resistances were

Table IV. Comparison of Various Resistances (Pressure: 100 kPa and Initial BSA Concentration: 1000 mg L^{-1})

Molecular wt. of PVP	pH	$R_t \times 10^{-13}$ (m^{-1})	R_m/R_t (%)	R_g/R_t (%)	R_r/R_t or R_{pb}/R_t (%)
24,000	9.3	3.12	27.32	43.16	29.52
	7	2.32	24.99	34.80	40.21
	4.8	8.69	25.48	52.21	22.31
40,000	9.3	4.44	20.54	49.21	30.25
	7	3.85	18.36	47.04	34.60
	4.8	14.28	25.41	38.34	36.25
360,000	9.3	5.26	29.95	29.80	40.25
	7	4.33	21.51	50.37	28.12
	4.8	22.33	35.56	26.20	38.24

calculated using Eqs. (15–17). Table IV shows resistances at different pH after 2 h of operation. It has been observed that total resistance was highest at pH 4.8 (i.e., IEP of BSA) irrespective to the molecular weight of PVP, it may be due the reason that the BSA is least soluble at its IEP and hence concentration of BSA molecules was highest on the surface of the membranes. Membrane hydraulic resistance was lowest at pH 7 (i.e., neutral condition) for all the membranes. Pore blocking resistance was varying because the average size of pores on the surface of membranes was different and was smallest for PSF_3.

CONCLUSION

Flat sheet PSF membranes were fabricated from casting solutions containing NMP as solvent with 14 wt % of PSF, by means of diffusion-induced phase separation process. PVP of average molecular weights of 24,000 Da, 40,000 Da, and 360,000 Da and PAA molecular weight of 18,000 Da were taken as additives. Effects of molecular weight of PVP with constant molecular weight of PAA on the morphology such as porosity in terms of average pore size, pore number and pore area were investigated in detail. The permeation behavior of the prepared membranes with varying molecular weight of PVP with PAA was examined in terms of EWC, PWF, CF, hydraulic permeability, and rejection efficiency of BSA protein. Contact angle was measured, for evaluation of the hydrophilicity of different prepared membranes. The SEM photographs show that all the membranes contain porous asymmetric structure. The results were compared with Chakrabarty *et al.*[23] So, with increasing molecular weight of PVP observations may be summarized as follows:

i. The number of pores per unit surface area (porosity) of the prepared membranes was found to be increased.
ii. The hydraulic resistance increased while PWF decreased possibly due to comparatively more compact structure of the resulting membranes and swelling of hydrophilic PVP–PAA molecule which remains entangle in the membrane matrix.
iii. The EWC increased which might be depicted as indication of increase in hydrophilicity (which was also confirmed by contact angle measurement) and number of pores of the membranes.
iv. Increase in rejection and as a result decrease in flux was observed in BSA separation. Further rejection of BSA was found more irrespective of the molecular weight of PVP at pH 4.8 (IEP of BSA). Highest rejection was observed as 87.5% by PSF_3 membrane at pH 4.8. Reversible fouling (R_r), irreversible fouling (R_{ir}), and then total fouling (R_t) were also measured and it was found that value of R_t was raised with molecular weight of PVP. Overall, all three membranes were found better than Chakrabarty *et al.*[23] in all aspects such as EWC (%), hydraulic resistance, R_m (m^2 h kPa L^{-1}), PWF, CF, BSA rejection (%) at pH 9.3, average radius of pore, r_{av} (nm), number of pores, N_t (cm^2), and area of pores, A_t (cm^2).

Finally, it may be concluded that the addition of PAA with PVP in casting solution can give better results than addition of PVP alone.

NOMENCULATURE

List of symbols

A	effective membrane area (m^2)
AFM	atomic force microscopy
A_t	total area
BSA	bovine serum albumin
CA	cellulose acetate
CF	compaction factor
C_{HCl}	concentration of HCl solution (M)
C_f	concentration in the feed in mg mL^{-1}
C_p	concentration in the permeate in mg mL^{-1}
d_p	diameter of pore
EWC	equilibrium water content
FESEM	field-emission scanning electron microscope
IEC	ion exchange capacity
IEP	isoelectric point
J_p	BSA solution flux (L m^{-2} h^{-1})
J_w	pure water flux (L m^{-2} h^{-1})
J_{w1}	initial water flux (L m^{-2} h^{-1})
J_{w2}	water flux in second run (L m^{-2} h^{-1})
L_n	total hydraulic permeability coefficient
l_p	length of pores
M	molarity
MF	microfiltration
NF	nanofiltration
N	number of pores
$N_{i,j}$	number of pores having radius between r_i and r_j
NMP	N-methyl-2-pyrrolidone
NP	nanoparticle
N_t	total number of pores per unit area of membrane
P	transmembrane pressure (kPa)
$\triangle P$	pressure difference
P_T	pressure
PAA	polyacrylic acid
PAN	polyacrylonitrile
PE	polyethylene
PEG	polyethylene glycol
PEGME	polyethylene glycol methyl ether
PES	polyethersulfone
P_m	hydraulic permeability (L m^{-2} h^{-1} kPa^{-1})
PP	polypropylene
PSF	polysulfone
PVDF	polyvinylidene fluoride
PVP	polyvinylpyrrolidone
PWF	pure water flux
Q	volume of water permeated (L)
r	radius of pores
R_g	gel layer resistance
R_{ir}	irreversible fouling
R_m	membrane resistance
RO	reverse osmosis
R_{PB}	resistance due to pore blocking
R_r	reversible fouling
R_t	total fouling
$\triangle t$	permeation time
UF	ultrafiltration

V	volume of membrane in wet state
Vb	consumed volumes of the NaOH solution for the blank sample (L)
Vs	consumed volumes of the NaOH solution for the PSF–(PVP–PAA) membrane sample (L)
W_d	weight of dry membrane
W_w	weight of wet membrane
W_{dry}	mass of dry membrane sample (g)

Greek letters

ε_m	surface porosity of membrane
μ	liquid viscosity
τ	pore tortuosity
ρw	density of water

ACKNOWLEDGMENTS

This work is partially supported by a grant from the Indian National Science Academy (INSA), New Delhi. Any opinions, findings and conclusions expressed in this article are those of the authors and do not necessarily reflect the views of INSA, New Delhi.

REFERENCES

1. Reis, R. V.; Zydney, A. *Curr. Opin. Biotechnol.* **2001**, *12*, 208.
2. Li, Q.; Bi, Q.; Lin, H.; Bian, L.; Wang, X. *J. Membr. Sci.* **2013**, *427*, 155.
3. Bruggen, B. V.; Curcio, E.; Drioli, E. *J. Env. Manag.* **2004**, *73*, 267.
4. Prifti, H.; Parasuraman, A.; Winardi, S.; Lim, T. M.; Skyllas-Kazacos, M. *Membranes* **2012**, *2*, 275.
5. Fahnestock, K. J.; Austero, M. S.; Schauer, C. L. *Biopolym. Biomed. Env. Appl.* **2011**, doi:10.1002/9781118164792.ch3.
6. Kariduraganavar, M. Y.; Nagarale, R. K.; Kittur, A. A.; Kulkarni, S. S. *Desalination* **2006**, *197*, 225.
7. Mulder, M. Basic Principles of Membrane Technology; Kluwer Academic Publishers: Dordrecht, **1991**.
8. Zhang, Y.; Shana, L.; Tua, Z.; Zhang, Y. *Sep. Purif. Technol.* **2008**, *63*, 207.
9. Kim, E. S.; Yu, Q.; Deng, B. *Appl. Surf. Sci.* **2011**, *257*, 9863.
10. Dattatray, S.; Wavhal, E. R.; Fisher, E. R. *Desalination* **2005**, *172*, 189.
11. Zhaoa, Y. F.; Zhua, L. P.; Yia, Z.; Zhua, B. K.; Xu, Y. Y. *J. Membr. Sci.* **2013**, *440*, 40.
12. Isloor, A. M.; Ganesh, B. M.; Isloor, S. M.; Ismail, A. F.; Nagaraj, H. S.; Pattabi, M. *Desalination* **2013**, *308*, 82.
13. Susanto, H.; Ulbricht, M. *Langmuir* **2007**, *23*, 7818.
14. Belfer, S.; Gflron, J.; Purinson, Y.; Fainshtain, R.; Daltrophe, N.; Priel, M.; Tenzer, B.; Toma, A. *Desalination* **2001**, *139*, 169.
15. Hester, J. F.; Banerjee, P.; Mayes, A. M. *Macromolecules* **1999**, *32*, 1643.
16. Qiu, S.; Wu, L. G.; Pan, X. J.; Zhang, L.; Chen, H. L.; Gao, C. J. *J. Membr. Sci.* **2009**, *342*, 165.
17. Nair, A. K.; Isloor, A. M.; Kumar, R.; Ismail, A. F. *Desalination* **2013**, *322*, 69.
18. Razmjou, A.; Mansouri, J.; Chen, V. *J. Membr. Sci.* **2011**, *378*, 73.
19. Bowen, W. R.; Doneva, T. A.; Yin, H. B. *J. Membr. Sci.* **2001**, *181*, 253.
20. Puasa, S. W.; Ruzitah, M. S.; Sharifah, A. S. K. International Conference on Environment and Industrial Innovation IPCBEE, **2011**; Vol. 12.
21. Sinha, M. K.; Purkait, M. K. *J. Membr. Sci.* **2013**, *437*, 7.
22. Chakrabarty, B.; Ghoshal, A. K.; Purkait, M. K. *J. Membr. Sci.* **2008**, *309*, 209.
23. Chakrabarty, B.; Ghoshal, A. K.; Purkait, M. K. *J. Membr. Sci.* **2008**, *315*, 36.
24. Chun, M. K.; Cho, C. S.; Choi, H. K. *J. Appl. Polym. Sci.* **2004**, *94*, 2390.
25. Kamusewitz, H.; Tiedemann, M. S.; Keller, M.; Paul, D. *Surf. Sci.* **1997**, *377–379*, 1076.
26. Hand, A. J.; Sun, T.; Barber, D. C.; Hose, D. R.; MacNeil, S. *J. Microsc.* **2009**, *234*, 62.
27. Horcas, I.; Fernandez, R.; Gomez-Rodriguez, J. M.; Colchero, J.; Gomez-Herrero, J.; Baro, A. M. *Rev. Sci. Instrum.* **2007**, *78*, 013705.
28. Cappanelli, G.; Vigo, F.; Munari, S. *J. Membr. Sci.* **1983**, *15*, 289.
29. Farbod, M.; Rezaian, S. *Thin Solid Films* **2012**, *520*, 1954.
30. Higuchi, A.; Ishida, Y.; Nakagawa, T. *Desalination* **1993**, *90*, 127.
31. Wang, T. Y. Q.; Wang, Y.; Su, F.; Wu, H. P.; Jiang, Z. *Langmuir* **2005**, *21*, 11856.
32. Yan, X.; He, G.; Gu, S.; Wua, X.; Dua, L.; Wanga, Y. *Int. J. Hydrogen Energy* **2012**, *37*, 5216.
33. Cheryan, M. Ultrafiltration and Microfiltration Handbook; CRC Press: FL, **1998**.
34. Kimmerle, K.; Strathmann, H. *Desalination* **1990**, *79*, 283.
35. Reuvers, J.; Smolders, C. A. *J. Membr. Sci.* **1987**, *34*, 67.
36. Machado, P. S. T.; Habert, A. C.; Borges, C. P. *J. Membr. Sci.* **1999**, *155*, 171.
37. Wienk, I. M.; Boom, R. M.; Beerlage, M. A. M.; Bulte, A. M. W.; Smolders, C. A. *J. Membr. Sci.* **1996**, *113*, 361.
38. Feng, C.; Wang, R.; Shi, B.; Li, G.; Wu, Y. *J. Membr. Sci.* **2006**, *277*, 55.
39. Sivakumar, M.; Malaisamy, R.; Sajitha, C. J.; Mohan, D.; Mohan, V.; Rangarajan, R. *Eur. Polym. J.* **1999**, *35*, 1647.
40. Young, T. H.; Chen, L. W. *J. Membr. Sci.* **1991**, *59*, 169.
41. Fane, A. G.; Fell, C. J. D.; Waters, A. G. *J. Membr. Sci.* **1981**, *9*, 245.
42. Musale, D. A.; Kulkarni, S. S. *J. Membr. Sci.* **1997**, *136*, 13.
43. Ghosh, R.; Cui, Z. F. *J. Membr. Sci.* **1998**, *139*, 17.
44. Sinha, M. K.; Purkait, M. K. *J. Membr. Sci.* **2014**, *464*, 20.
45. Hunter, R. J. Zeta Potential in Colloid Science; Academic Press: London, **1981**.